Online Set-Point Estimation for Feedback-Based Traffic Control Applications

Farzam Tajdari and Claudio Roncoli

***Abstract*— This paper deals with traffic control at motorway bottlenecks assuming the existence of an unknown, time-varying, Fundamental Diagram (FD). The FD may change over time due to different traffic compositions, e.g., light and heavy vehicles, as well as in the presence of connected and automated vehicles equipped with different technologies at varying penetration rates, leading to inconstant and uncertain driving characteristics. A novel methodology, based on Model Reference Adaptive Control, is proposed to robustly estimate in real-time the time-varying set-points that maximise the bottleneck throughput, particularly useful when the traffic is regulated via a feedback-based controller. Furthermore, we demonstrate the global asymptotic stability of the proposed controller through a novel Lyapunov analysis. The effectiveness of the proposed approach is evaluated via simulation experiments, where the estimator is integrated into a feedback ramp-metering control strategy, employing a second-order multi-lane macroscopic traffic flow model, modified to account for time-varying FDs.**

***Index Terms*— Traffic control, adaptive control, time-varying fundamental diagram, robust estimation.**

I. Introduction

TRANSPORT networks constitute the backbone of our society, enabling the mobility of people and the distribution of goods. However, due to urbanisation and suboptimal mobility policies and choices, transport infrastructures in and around metropolitan areas are reaching their saturation, with negative effects such as ever-increasing traffic congestion. This causes an increased need for energy, risk of accidents, traffic jams, and driver frustration [1], [2], [3]. In traffic networks, congestion is typically triggered by the activation of a bottleneck, which occurs when the traffic demand exceeds the road supply. In particular, in a motorway context, whenever there are lane drops, uphills, or curvatures, a bottleneck may appear, which, if activated, may produce a capacity drop, i.e., a reduction of the total discharging flow rate from the bottleneck area, causing travel time delay for the upstream traffic. Traffic congestion then propagates upstream of the bottleneck, until a significant reduction of the demand flow occurs [4], [5], [6].

A successful countermeasure able to mitigate or avoid the effects of congestion is traffic control, which consists in using some technological device (e.g., traffic signal, variable message sign, etc.) to regulate the flow entering a specific road area by employing some traffic measurement [7], [8]. Among other approaches, over the last decades, feedback-based traffic control methods have been proposed and sometimes implemented, able to partially deal with the aforementioned challenges.

In the context of feedback-based freeway traffic control, several recent studies have introduced different tools and investigated their impact in different traffic scenarios. The problem of controlling freeway traffic via isolated or coordinated ramp-metering methodologies has been tackled in several works, including [9], [10], [11], and [12]; another control strategy, variable speed limits, have been investigated in isolation or jointly with ramp-metering (see, e.g., [13], [14]); as well as in the context of mixed traffic with automated vehicles (see, e.g., [15], [16], [17]). Other control strategies, such as speed control has been investigated, e.g., in [18] and [19].

To investigate uncertainty in Fundamental Diagram (FD) related parameters, the work in [20] introduced a robust control method to deal with the uncertainties associated with the turning ratio by employing distributionally robust chance constraints. Later, the uncertainty in the assumption of a fixed FD, i.e., initial conditions and the model parameters resulting while a controller is implemented is studied in [21].

Despite their design peculiarities, all those control approaches require the knowledge of some features characterising the traffic behaviour in order to work effectively, which include the traffic capacity (i.e., maximum flow able to pass a bottleneck location) and the critical density or occupancy (i.e., the density or occupancy at which capacity occurs). These quantities are not trivial to obtain or estimate and they require the collection and analysis of traffic data for each area where traffic control is to be applied. Moreover, even once these parameters are calibrated, they may require constant tuning due to short- and long-term changes in traffic behaviour and characteristics. This will be amplified with the appearance of vehicle automation [22]; in fact, it is expected that vehicles with various driving assistance systems, such as Connected and Automated Vehicles (CAVs) are going to co-exist for the next decades, altering the current traffic characteristics and affecting the need for traffic control [23], [24], [25], [26].

Manuscript received 30 June 2022; revised 29 November 2022, 17 February 2023, and 29 March 2023; accepted 3 May 2023. Date of publication 16 May 2023; date of current version 4 October 2023. This work was supported in part by the Academy of Finland Project ULTRA under Grant 328216, in part by the Academy of Finland Project ALCOSTO under Grant 349327, and in part by the FINEST Twins Center of Excellence through the European Union Horizon 2020 programme under Grant 856602. The Associate Editor for this article was J. Xun. *(Corresponding author: Farzam Tajdari.)*

Farzam Tajdari is with the Department of Built Environment, School of Engineering, Aalto University, 02150 Espoo, Finland, and also with the Department of Mechanical Engineering, Dynamics and Control (D&C) Group, Technical University of Eindhoven, 5612 AZ Eindhoven, The Netherlands (e-mail: farzam.tajdari@aalto.fi).

Claudio Roncoli is with the Department of Built Environment, School of Engineering, Aalto University, 02150 Espoo, Finland (e-mail: claudio.roncoli@aalto.fi).

Digital Object Identifier 10.1109/TITS.2023.3274233

A way to deal with this issue is to design and employ adaptive estimation algorithms to automatically tune the parameters (e.g., the set-points) within control strategies. This has been proposed, e.g., in the context of urban traffic control, in [27] and [28], where the set-points are tuned on a day-to-day basis. Papers [29] employed a methodology based on discrete-time Extremum Seeking (ES), which is a model-free method, applied to traffic data for real-time optimisation, which has been broadly investigated and utilized in several applications, including, e.g., [30] and [28].

However, even if a set-point is estimated using offline data, it may not always be optimal because of possible real-time changes in traffic behaviour characteristics, which implies the importance of online identification of the set-point [31]. The change in traffic characteristics may be caused, by a different traffic composition (e.g., of trucks and cars) or by the presence of CAVs at various penetration rates. However, online estimation of the FD for full AV or mixed human-driven and AV traffic is relatively scarce in the literature [32]. To our best knowledge, the only existing works dealing simultaneously with control and online set-point estimation are [33] and [34]. The work in [33] employs a method proposed in [35], developing an online ES control approach to calculate the optimal density input for motorway traffic, when there is a downstream bottleneck. However, such an approach is restricted to a single lane with a one-link network, while the slow convergence speed of the algorithm makes it unsuitable for practical applications. In [34], two methods, i.e., Simple Derivative Estimation and Kalman Filter–based Estimation algorithms, are compared to estimate set-points for a ramp-metering application; however, the methods suffer in the case of strong short-term changes of the actual set-point value, while being sensitive to the changes of the traffic flow parameters, which require significant off-line fine-tuning of the methods' parameters.

Apart from the approaches mentioned above, there exist methods capable of simultaneously controlling and identifying the unknown parameters of a system online (see, e.g., [36]). One suitable method is Model Reference Adaptive Control (MRAC), which is designed to exploit conventional controllers while the controllers' parameters are updated based on model parameters identification, where the model structure is assumed known and parameter values are unknown. Such methods have been widely used, e.g., in controlling robotic systems [37], online identification [38], [39], and noise filtering [40]. In the field of traffic control, Haddad et al. [41] presented a two-stage framework based on MRAC as an extension to [42] that i) incorporates state delay in a Macroscopic Fundamental Diagram (MFD), and ii) employs them to model data processing and communication delays between interconnected regions. The work in [43] presents a unified methodology extending [44], which exploits MRAC to adaptively compensate input delays, which can be constant, time-varying, or dependent on the current plant state while taking into account the effect of control saturation. Although employing such adaptive control methods has considerable potential in the domain of traffic control, there is a lack of literature on designing and testing such control schemes that aim at identifying traffic flow parameters.

This paper proposes an adaptive control scheme consisting of a novel globally robust MRAC-based approach for estimating constant or time-varying unknown set-points (in the form of critical densities) for controlling a local motorway bottleneck, to maximise the outflow and, consequently, reducing travel delays. Our main scientific contributions are as follows.

- We propose an adaptive dynamic set-point (critical density) estimator, assuming the availability of local traffic measurements, such as the traffic density and flow at the bottleneck.
- We prove that the estimator error dynamic is globally asymptotically and exponentially stable via a novel Lyapunov analysis.
- We perform numerical investigations employing a state-of-the-art traffic control strategy and non-linear traffic model, to demonstrate the effectiveness of the proposed method. Furthermore, we perform numerical analyses to demonstrate the robustness against parameter choices and disturbances.

A preliminary version of this work has been proposed in [45], which, however, suffers from some limitations elaborated as follows. The adaptation rule for updating the estimating parameters is designed via a Lyapunov function that guarantees only conditional stability, while it is not proven whether the designed growth rate parameter is able to guarantee the convergence of the estimates to the true values. Furthermore, the designed growth rate may lead to slow estimation and large delays when the unknown parameters undergo fast changes. Accordingly, the work in [45] is extended here in various aspects. First, we provide a novel formulation of the adaptive estimator, demonstrating its global asymptotic stability, which guarantees true value identification of the unknown parameters. Second, we incorporate a methodology for online tuning of its growth-rate parameters, while also thoroughly investigating the stability properties of the proposed adaptive estimation law. Third, we redesign the numerical experiments by considering state-of-the-art modelling and control strategies, while investigating also the robustness of parameter choices.

II. Adaptive Estimator Design

A. Preliminary

Here, we introduce the fundamentals for establishing an estimator that allows a feedback controller to maximise the outflow at a motorway bottleneck. As, due to less pronounced fluctuations, it is preferable to employ density as a set-point for the controller [46], the problem reduces to estimating the critical density at the motorway bottleneck. To this end, we begin by explaining our main assumptions; then, we elaborate on the controller design; finally, we demonstrate the convergence of the estimated values and the stability of the proposed approach.

For the design of the estimator, we formulate a parabolic flow-density ($q-\rho$) relationship, denoted as FD; note however that we will demonstrate in Section IV that the approach is

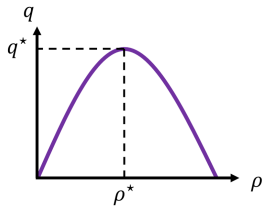

Fig. 1. The FD shape assumed at the bottleneck area.

also effective when a different shape for the FD is employed, as long as it is concave and features a unique maximum point.

In particular, we employ the following function describing the FD, also depicted in Fig. 1,

$$q = a\rho^2 + b\rho, \tag{1}$$

where a and b are unknown parameters; function (1) has a maximum point $(\rho^\star, q^\star)$ as

$$\rho^\star = \frac{-b}{2a}, \quad q^\star = \frac{-b^2}{4a}; \tag{2}$$

note that $q^\star$ is the maximum flow (capacity) and $\rho^\star$ is the critical density.

B. Adaptive Estimator Design

By replacing the nominal values of $q^\star$ and $\rho^\star$ in (1), the error of q from $q^\star$ is

$$q - q^\star = a(\rho^2 - \rho^{\star 2}) + b(\rho - \rho^\star). \tag{3}$$

Now, we introduce the integral error states

$$E_q = \int \left(q - q^\star\right) dt \tag{4}$$

$$E_\rho = \int \left(\rho - \rho^\star\right) dt, \tag{5}$$

allowing to define the integral error system

$$\dot{E}_q = q - q^\star \tag{6}$$

$$\dot{E}_\rho = \rho - \rho^\star, \tag{7}$$

that can be reformulated as

$$\dot{X} = B_e u_e + r_e, \tag{8}$$

where

$$X = \begin{bmatrix} \int q\ dt \\ \int \rho\ dt \end{bmatrix}, \quad u_e = \begin{bmatrix} u_1 \\ u_2 \end{bmatrix} = \begin{bmatrix} \rho^{\star 2} - \rho^2 \\ \rho - \rho^\star \end{bmatrix} \tag{9}$$

$$B_e = \begin{bmatrix} -a & b \\ 0 & 1 \end{bmatrix}, \quad r_e = \begin{bmatrix} q^\star \\ \rho^\star \end{bmatrix}. \tag{10}$$

We propose controlling system (8) using MRAC [36], which let us simultaneously identify the unknown parameters a and b (both appearing in B_e) and minimise the tracking error. In order to proceed, we introduce the feedback control law (see, e.g., Chapter 1 in [47])

$$u_e = -\hat{\Pi}(X - r_e), \tag{11}$$

where $\hat{\Pi}$ is an unknown matrix that needs to be estimated. We rewrite (11) as

$$u_e = \hat{\Pi}\ \bar{I} v, \tag{12}$$

where $\bar{I} = \begin{bmatrix} -I_{2\times 2} & I_{2\times 2} \end{bmatrix}$ ($I_{2\times 2}$ is the identity matrix) and $v = \begin{bmatrix} X \\ r_e \end{bmatrix}$. We then introduce a model reference

$$\dot{X}_M = -A_M X_M + B_M r_e, \tag{13}$$

where A_M and B_M are arbitrarily defined matrices that guarantee a stable model reference dynamics. Let us define the error between the integral states and the model reference $e = X - X_M$, whose dynamics are defined as (see [36])

$$\begin{aligned} \dot{e} &= \dot{X} - \dot{X}_M \\ &= B_e(-\hat{\Pi}X + \hat{\Pi}r_e) + r_e + A_M X_M - B_M r_e + A_M X - A_M X \\ &= -A_M(X - X_M) + B_e(-\hat{\Pi} + A_M)X + B_e(\hat{\Pi} - \frac{B_M - I}{B_e})r_e \\ &= -A_M e + B_e(-\hat{\Pi} + A_M)X + B_e(\hat{\Pi} - \frac{B_M - I}{B_e})r_e, \end{aligned} \tag{14}$$

which, converting to the Laplace domain, leads to

$$\begin{aligned} e &= \frac{B_e}{sI + A_M}\left[-\hat{\Pi} + \frac{A_M}{B_e} \middle| \hat{\Pi} - \frac{B_M - I}{B_e} \right] v \\ &= \frac{\bar{B}_e}{sI + A_M}\left[-\hat{\Pi}\Theta(B_e) + \frac{A_M}{\bar{B}_e} \middle| \hat{\Pi}\Theta(B_e) - \frac{B_M - I}{\bar{B}_e} \right] v, \end{aligned} \tag{15}$$

where s is the Laplace variable, and Θ is a sign operator defined as follows

$$\Theta(i) = \begin{cases} 1, & \text{if } i > 0 \\ 0, & \text{if } i = 0 \\ -1, & \text{if } i < 0. \end{cases} \tag{16}$$

We can observe that the error dynamics of (15) is stable over time if and only if changes of $\hat{\Pi}$ are restricted to a finite domain or $\hat{\Pi}$ is converging to a certain value (see Section II-C), considering that $-A_M$ is selected as a stable matrix with negative eigenvalues, while B_M and B_e are constant matrices. As the term $\Theta(B_e)$ appears in (15), to facilitate the calculation we rewrite (12) as

$$u_e = \Theta(B_e)\hat{\Pi}\ \bar{I} v; \tag{17}$$

then, by replacing (17) into (8), we obtain

$$\dot{X} = B_e\Theta(B_e)\hat{\Pi}\ \bar{I} v + r_e, \tag{18}$$

which, defining $\bar{B}_e = B_e\Theta(B_e)$, results in

$$\dot{X} = -\bar{B}_e\hat{\Pi}X + \left(\bar{B}_e\hat{\Pi} + I\right) r_e. \tag{19}$$

System (19) is exponentially stable around r_e if $\lim_{t\to\infty} \hat{\Pi} \to \bar{B}_e$, as $-\bar{B}_e\hat{\Pi}$ is a Hurwitz matrix (see Chapter 3 in [48]).

C. Derivation of the Estimation Law

In order to derive the estimation law, we start by studying the convergence of $\tilde{\Pi} = \hat{\Pi} - \Pi$, by employing the following exponential Lyapunov function

$$\mathcal{V} = X\mathcal{P}X^{\mathrm{T}} + \tilde{M}^{\mathrm{T}}\Gamma^{-1}\tilde{M} \tag{20}$$

$$\bar{\mathcal{V}} = \exp(-\gamma\mathcal{V}), \tag{21}$$

where we define $\tilde{M} = \exp(\beta|\tilde{\Pi}|)$. Denoting $\hat{M} = \exp(\pm\,\beta\hat{\Pi})$ and $M = \exp(\mp\,\beta\Pi)$, then $\tilde{M} = \exp(\pm\beta\hat{\Pi})\exp(\mp\beta\Pi)$ and, since Π is assumed constant ($\dot{\Pi} = 0$), M is a constant positive matrix in (21) that can be neglected, which leads us to

$$\tilde{M} = \exp(\beta|\hat{\Pi}|). \tag{22}$$

Furthermore, having $\mathcal{P} \geq 0$ (scalar), $\gamma > 0$ (scalar), $\beta > 0$ (scalar), and $\Gamma > 0$ (matrix), leads to $\bar{\mathcal{V}} > 0$. For achieving exponential global stability, it is sufficient that $\dot{\bar{\mathcal{V}}} \leq -\bar{\mathcal{V}}$ (see, e.g., [48], [49]); then

$$\dot{\bar{\mathcal{V}}} = -\gamma\bar{\mathcal{V}}\frac{d\mathcal{V}}{dt} \leq -\bar{\mathcal{V}} \tag{23}$$

and, since γ and $\bar{\mathcal{V}}$ are always positive, the sufficient condition reduces to

$$\frac{d\mathcal{V}}{dt} \geq \frac{1}{\gamma}I, \tag{24}$$

thus

$$\frac{d\mathcal{V}}{dt} = \dot{X}\mathcal{P}X^{\mathrm{T}} + X\mathcal{P}\dot{X}^{\mathrm{T}} + \dot{\tilde{M}}^{\mathrm{T}}\Gamma^{-1}\tilde{M} + \tilde{M}^{\mathrm{T}}\Gamma^{-1}\dot{\tilde{M}}. \tag{25}$$

By obtaining u_e^{T} from (17) and replacing it into (25), we obtain

$$\frac{d\mathcal{V}}{dt} = 2PB_eXv^{\mathrm{T}}\bar{I}^{\mathrm{T}}\hat{\Pi}^{\mathrm{T}}\Theta(B_e)^{\mathrm{T}} + 2\dot{\tilde{M}}^{\mathrm{T}}\Gamma^{-1}\tilde{M}. \tag{26}$$

Defining $\mathcal{P}B_e = C$, $e = CX$, and combining (24) and (26) we obtain the condition

$$2\dot{\tilde{M}}^{\mathrm{T}}\Gamma^{-1}\tilde{M} + 2\,ev^{\mathrm{T}}\bar{I}^{\mathrm{T}}\hat{\Pi}^{\mathrm{T}}\Theta(B_e)^{\mathrm{T}} = \frac{1}{\gamma}I, \tag{27}$$

which, by replacing $\dot{\tilde{M}} = \beta\tilde{M}\,\Theta(\hat{\Pi})\dot{\hat{\Pi}}$, results in

$$\beta\dot{\hat{\Pi}}^{\mathrm{T}}\Gamma^{-1}\Theta(\hat{\Pi})^{\mathrm{T}}\tilde{M}^{\mathrm{T}}\tilde{M} = \frac{1}{2\gamma}I - ev^{\mathrm{T}}\bar{I}^{\mathrm{T}}\hat{\Pi}^{\mathrm{T}}\Theta(B_e)^{\mathrm{T}}. \tag{28}$$

That is, as long as the condition in (28) is satisfied and $\gamma > 0$, $\hat{\Pi}$ is converging. Moreover, we define $\frac{1}{\gamma}I = 0^{+}_{2\times 2}$, which results in

$$\beta\dot{\hat{\Pi}}^{\mathrm{T}}\Gamma^{-1}\Theta(\hat{\Pi})^{\mathrm{T}}\tilde{M}^{\mathrm{T}}\tilde{M} = -ev^{\mathrm{T}}\bar{I}^{\mathrm{T}}\hat{\Pi}^{\mathrm{T}}\Theta(B_e)^{\mathrm{T}}; \tag{29}$$

thus, a sufficient condition for stability is that the changes in the unknown parameters are

$$\dot{\hat{\Pi}}^{\mathrm{T}} = -ev^{\mathrm{T}}\bar{I}^{\mathrm{T}}\frac{\hat{\Pi}^{\mathrm{T}}\Theta(\hat{\Pi})^{\mathrm{T}}}{\tilde{M}^{\mathrm{T}}\tilde{M}}\Theta(B_e)^{\mathrm{T}}\frac{1}{\beta}\Gamma, \tag{30}$$

where Γ is known as the *growth rate* of the estimation law. Assuming $\Gamma^{\mathrm{T}} = \Gamma$, $\Theta(\hat{\Pi})\hat{\Pi} = |\hat{\Pi}|$, and $\mathcal{R}_{2\times 2} = \frac{1}{\beta}\Theta(B_e)\frac{|\hat{\Pi}|}{\tilde{M}^{\mathrm{T}}\tilde{M}}$, this results in the adaptation law

$$\dot{\hat{\Pi}} = -\Gamma\mathcal{R}\bar{I}ve^{\mathrm{T}}. \tag{31}$$

Remark 1: Regarding (31), it should be noted that the term $\frac{|\hat{\Pi}|}{\tilde{M}^{\mathrm{T}}\tilde{M}}$ includes $\tilde{M}$ in its denominator, which may lead to instability. However, from (22), we know that $\tilde{M} \geq 1$, which prevents the occurrence of a singularity. In addition, by plotting a scalar version of such a term (refer to Fig. 2), one can observe that a) the term is well-bounded and b) if $\hat{\Pi}$ becomes very large, the term $\frac{|\hat{\Pi}|}{\tilde{M}^{\mathrm{T}}\tilde{M}} \to 0$, which, in turn, results in the boundedness of $\hat{\Pi}$, still satisfying the asymptotic stability of the error system in (14).

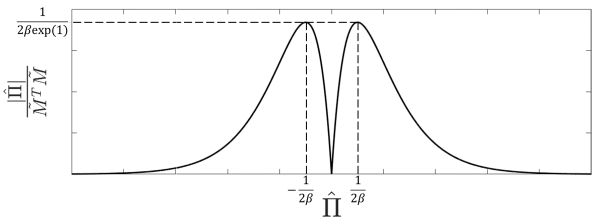

Fig. 2. Schematical behaviour of the nonlinear term $\frac{|\hat{\Pi}|}{\tilde{M}^{\mathrm{T}}\tilde{M}}$ in (31) for the case where $\hat{\Pi}$ is a scalar.

D. The Growth Rate of the Estimator

Although any positive constant value for Γ is theoretically sufficient to guarantee the global stability of the estimation scheme, it may not guarantee the global asymptotic stability of the estimation error (i.e., $\hat{\Pi} \to \Pi$). To address this shortcoming, we redefine Γ as a time-varying parameter, considering that the tracking error for system (8) is $\bar{e} = X - r_e$; this leads to

$$\Gamma(t) = \left(\int_0^t \mathcal{R}\bar{e}(r)\bar{e}^{\mathrm{T}}(r)dr\right)^{-1}, \tag{32}$$

where

$$\frac{d}{dt}\left(\Gamma^{-1}(t)\right) = \mathcal{R}\bar{e}(t)\bar{e}^{\mathrm{T}}(t). \tag{33}$$

From (31), knowing that $e^{\mathrm{T}}(t) = \bar{e}^{\mathrm{T}}(t)(\Pi - \hat{\Pi})$ and $\bar{I}v(t) = r_e - X = -\bar{e}(t)$, we have that

$$\dot{\hat{\Pi}} = \Gamma\mathcal{R}\bar{e}(t)\bar{e}^{\mathrm{T}}(t)(\Pi - \hat{\Pi}) \tag{34}$$

$$\Gamma^{-1}(t)\,\dot{\hat{\Pi}} + \mathcal{R}\bar{e}(t)\bar{e}^{\mathrm{T}}(t)\,\hat{\Pi} = \mathcal{R}\bar{e}(t)\bar{e}^{\mathrm{T}}(t)\Pi \tag{35}$$

$$\frac{d}{dt}(\Gamma^{-1}(t)\hat{\Pi}) = \mathcal{R}\bar{e}(t)\bar{e}^{\mathrm{T}}(t)\Pi \tag{36}$$

$$\frac{d}{dt}\left(\int_0^t \mathcal{R}\bar{e}(r)\bar{e}^{\mathrm{T}}(r)dr\hat{\Pi}\right) = \mathcal{R}\bar{e}(t)\bar{e}^{\mathrm{T}}(t)\Pi \tag{37}$$

$$\int_0^t \mathcal{R}\bar{e}(r)(\bar{e}^{\mathrm{T}}(r)\hat{\Pi} - \bar{e}^{\mathrm{T}}(r)\Pi)dr = 0. \tag{38}$$

Essentially, (38) implies that the proposed estimation law is minimizing a cost function based on the well-known least-square method, with the cost function

$$J = \int_0^t ||\bar{e}^{\mathrm{T}}(r)\hat{\Pi} - \bar{e}^{\mathrm{T}}(r)\Pi||^2\,dr. \tag{39}$$

However, while implementing the estimator, it is desirable to update the gain $\Gamma(t)$ directly, rather than using (33) and then inverting the matrix Γ^{-1}, which may cause numerical issues. Instead, by using the identity matrix

$$\frac{d}{dt}\left(\Gamma(t)\Gamma^{-1}(t)\right) = \dot{\Gamma}(t)\Gamma^{-1}(t) + \Gamma(t)\frac{d}{dt}\left(\Gamma^{-1}(t)\right) = 0, \tag{40}$$

we obtain

$$\dot{\Gamma}(t) = -\Gamma(t)\mathcal{R}\bar{e}(t)\bar{e}^{T}(t)\Gamma(t). \tag{41}$$

While using (31) and (41) for online estimation, we need to specify initial values for the estimated parameters and the gain of growth rate. However, the initialisation may be challenging, as from (31) and (41) it results that $\Gamma(0)$ should be a very large value (theoretically approaching infinity), whereas $\hat{\Pi}$ is

initially undefined. To tackle this challenge, assuming proper finite values to initialize Γ and $\hat{\Pi}$ can be a problem solver. In fact, one should use the best guess to initialize $\hat{\Pi}$, a proper initial value of the gain $\Gamma(0)$ must be opted as high as allowed by the noise sensitivity extracted from the dynamic of the system analysis. Note that, for the sake of simplicity, $\Gamma(0)$ may be chosen as a diagonal matrix.

E. Parameter Convergence

Theoretically, the convergence properties of the estimator can be revealed via solving the differential equations (33) and (31), assuming the absence of noise and parameter variation. From (33), (31), and (41), one may see that

$$\Gamma^{-1}(t) = \Gamma^{-1}(0) + \int_0^t \mathcal{R}\bar{e}(r)\bar{e}^T(r)dr \tag{42}$$

$$\frac{d}{dt}\left(\Gamma^{-1}(t)\tilde{\Pi}(t)\right) = 0. \tag{43}$$

Assuming equilibrium conditions (i.e., $\dot{\Pi} = 0$), we obtain

$$\tilde{\Pi}(t) = \Gamma(t)\Gamma^{-1}(0)\tilde{\Pi}(0). \tag{44}$$

As $\bar{I}v = -\bar{e}$ if v is such that

$$\lim_{t\to\infty} \lambda_{\min}\left(\int_0^t \mathcal{R}\bar{e}(r)\bar{e}^T(r)dr\right) \to \infty \tag{45}$$

$$\lim_{t\to\infty} \lambda_{\min}\left(\int_0^t \mathcal{R}\bar{I}v(r)v^T(r)\bar{I}^{\mathrm{T}}dr\right) \to \infty \tag{46}$$

and knowing that when $t \to \infty$, $\mathcal{R}$ is a bounded constant matrix as a function of $\hat{\Pi}$, then (46) can be rewritten (by excluding the constant matrices) as follows

$$\lim_{t\to\infty} \lambda_{\min}\left(\int_0^t v(r)v^T(r)dr\right) \to \infty, \tag{47}$$

where $\lambda_{\min}(\cdot)$ denotes the smallest eigenvalue of its argument. The gain matrix converges to a small positive value and the estimated parameters asymptotically (although usually not exponentially) converge to the true parameters. Indeed, for any positive integer k,

$$\int_0^{k\sigma+\sigma} v(r)v^T(r)dr = \sum_{i=0}^{k}\int_{i\sigma}^{i\sigma+\sigma} !v(r)v^T(r)dr \geq k\alpha_1\ I. \tag{48}$$

Thus, if v is persistently excited, (48) is satisfied; then, according to [50] and [51], Γ converges to a small positive value and $\tilde{\Pi} \to 0$.

Note that the impact of the initial gain value and the initial parameter value on the estimation process is observable from (42), (43), and (44). In fact, a small error in the parameter's initialisation value ($\tilde{\Pi}(0)$), always leads to a small parameter estimation error. Whereas, a large initial gain $\Gamma(0)$ results in a small parameter estimation error. Generally, based on (32), Γ is a very small value and according to (41), it is exponentially converging to zero. Thus, if $\Gamma(0)$ is not big enough we may have no update or a very low-speed update in the parameter estimation. This is more evident if we select $\Gamma(0) = \Gamma_0 I$, which results in

$$\tilde{\Pi} = \left(I + \Gamma_0\int_0^t \mathcal{R}\bar{e}(r)\bar{e}^T(r)dr\right)^{-1}\tilde{\Pi}(0). \tag{49}$$

F. Robustness to Noise in the Density and Flow Measurement

Generally, the least-squares method (39) used for the designed growth rate (Γ) calculated via (41) performs robustly with respect to noise and disturbance. Proper noise-rejection capability results from the fact that noise, particularly if characterised by high frequency, is averaged out. The estimator's inability to track highly fluctuating parameters (different from switching parameters' values) is also intuitively understandable, from two different viewpoints. In mathematical terms, $\Gamma(t)$ converges to zero when v is persistently excited according to (43), i.e., the parameter update is essentially shut off after some time, and the changing parameters cannot be updated anymore. In practical terms, the least-square estimator tries to fit all the data up to the current time, while, in practice, the previous data is extracted by the previous parameters.

G. The Estimator Framework

The overall framework presented in this paper, shown in Fig. 3, includes a feedback controller designed to maintain the density at a motorway bottleneck around the critical set-point estimated via the proposed methodology. The framework is composed of three main parts: a) the feedback traffic control loop (grey part); b) the adaptive estimator (orange part), and c) the adaptive estimator's parameters (growth rate) estimation (green part). The grey part essentially includes any feedback controller that utilises density as a set-point to maximise bottleneck throughput. The orange part represents the estimation process of $\rho^\star$ and $q^\star$, while the growth rate of the estimator (Γ) is adaptively estimated as shown in the green part.

To implement the parameter estimation in discrete form, we consider $\dot{\hat{\Pi}}(k+1) = \frac{\hat{\Pi}(k+1)-\hat{\Pi}(k)}{\Delta t}$ and $\dot{\Gamma}(k+1) = \frac{\Gamma(k+1)-\Gamma(k)}{\Delta t}$ where Δt is time-step; then, the adaptation rule (31) and the gain update (41) turn into

$$\hat{\Pi}(k+1) = \hat{\Pi}(k) - \Delta t\left(\Gamma(k)\mathcal{R}(k)\bar{I}v(k)e(k)^{\mathrm{T}}\right), \tag{50}$$

$$\Gamma(k+1) = \Gamma(k) - \Delta t\left(\Gamma(k)\mathcal{R}(k)\bar{e}(k)\bar{e}^{\mathrm{T}}(k)\Gamma(k)\right). \tag{51}$$

The estimates $\hat{\rho}^\star$, namely the set-point for the feedback controller, can be obtained as (see (9))

$$\hat{\rho}^\star(k+1) = \rho(k+1) - u_2(k+1), \tag{52}$$

where u_2 is an element of u_e, which can be computed from $\hat{\Pi}$ and measured variables ρ. Moreover, the estimates for the maximum outflow $\hat{q}^\star$ is calculated as (see (9))

$$\hat{q}^\star(k+1) = -\frac{\hat{\Pi}^2_{1,2}(k+1)}{4\hat{\Pi}_{1,1}(k+1)}. \tag{53}$$

Note that (52) and (53) are defined so that we avoid having dependent parameter estimation, which is necessary to achieve convergence to the true values (see [36]).

III. Experimental Set-Up

We now proceed by demonstrating via numerical experiments the effectiveness of the proposed methodology. We first introduce the traffic simulation model and the feedback control ramp metering strategy considered in our experiments, followed by the evaluated scenarios and the parameters utilised for the model, controller, and estimator.

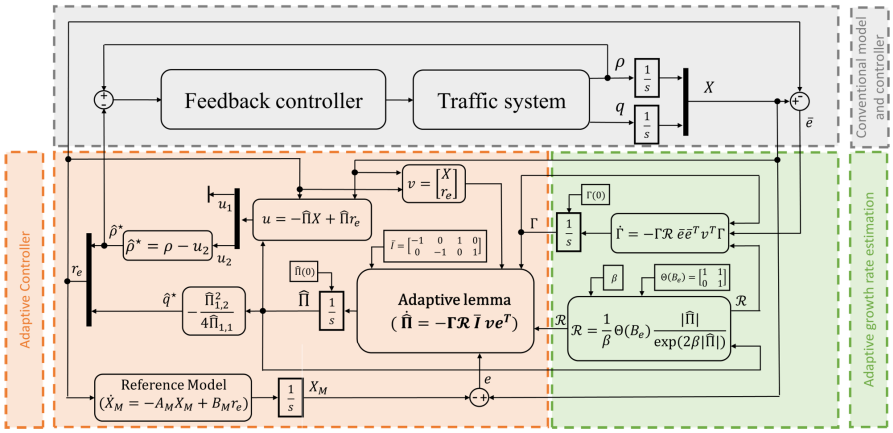

Fig. 3. Closed-loop diagram of the proposed estimation and control integrated framework.

A. The Macroscopic Traffic Flow Model METANET

The macroscopic traffic flow model METANET [52] is selected for the numerical experiments. METANET is a second-order traffic flow model consisting of two interconnected dynamic equations, which describe the evolution of traffic density and (space) mean speed, respectively. To define a space-time discretized model, the considered freeway stretch is subdivided into N cells of lengths L_i, $i = 1, 2, \ldots, N$; whereas the time $t = kT$ is discretized, where T is the simulation time step and $k = 0, 1, \ldots$ is the discrete-time index. The traffic characteristics of each cell are macroscopically identified by the following traffic variables:

- traffic density $\rho_i(k)$, as the number of vehicles in cell i at time $t = kT$, divided by L_i and by the number of lanes λ_i in the considered cell (measured in veh/km/lane);
- mean speed $v_i(k)$ as the mean speed of vehicles in cell i at time $t = kT$ (measured in km/h);
- traffic flow $q_i(k)$ as the number of vehicles leaving cell i during the time period $(kT, (k+1)T]$, divided by T (measured in veh/h).

The equations of the second-order macroscopic traffic flow model used to calculate the traffic variables are:

$$\rho_i(k+1) = \rho_i(k) + \frac{T}{L_i\lambda_i}\left[q_{i-1}(k) - q_i(k) + r_i(k) - s_i(k)\right] \tag{54}$$

$$\begin{aligned} v_i(k+1) = v_i(k) &+ \frac{T}{\tau}\left[V\left(\rho_i(k)\right) - v_i(k)\right] \\ &+ \frac{T}{L_i} v_i(k)\left[v_{i-1}(k) - v_i(k)\right] \\ &- \frac{\nu T}{\tau L_i}\frac{\rho_{i+1}(k) - \rho_i(k)}{\rho_i(k) + \kappa} - \frac{\delta T}{L_i\lambda_i}\frac{r_i(k)v_i(k)}{\rho_i(k) + \kappa} \end{aligned} \tag{55}$$

$$q_i(k) = \rho_i(k)v_i(k)\lambda_i \tag{56}$$

$$V\left(\rho_i(k)\right) = v_i^{\text{free}}(k)\exp\left[-\frac{1}{\alpha_i(k)}\left(\frac{\rho_i(k)}{\rho_i^{\text{cr}}(k)}\right)^{\alpha_i(k)}\right], \tag{57}$$

where τ (time constant), ν (anticipation constant), and κ (model parameter) are global parameters given for the whole motorway; $r_i(k)$ and $s_i(k)$ are the on-ramp inflow and off-ramp outflow, respectively; $V\left(\rho_i(k)\right)$ is a speed–density relationship that represents the FD; finally, $v_i^{\text{free}}(k)$ (free-flow speed), $\rho_i^{\text{cr}}(k)$ (critical density), and $\alpha_i(k)$ (model parameter) are parameters that characterise the FD in each cell, which, differently from the original formulation, in this work are considered time-dependent to describe the possibility of the FD to change over time. METANET is widely considered one of the most accurate macroscopic traffic models, capable of reproducing traffic instabilities and the capacity drop effect, which are essential for evaluating traffic control strategies.

B. ALINEA Ramp Metering Strategy

We assume traffic is controlled by the well-known ramp-metering feedback controller ALINEA [9]. The controller ALINEA is designed to maintain the total (cross-lane) density at its critical value in the bottleneck segment, which, in turn, is expected to maximise the bottleneck throughput. This is done by manipulating the ramp inflow via an I-type controller, according to the following control law

$$u(k) = u(k-1) + K_A\left(\hat{\rho}_{\hat{i}}^{\star}(k) - \rho_{\hat{i}}(k)\right), \tag{58}$$

where $u(k)$ is the controlled input (ramp flow); $\rho_{\hat{i}}(k)$ is the (measured) density at bottleneck cell $\hat{i}$; $\hat{\rho}_{\hat{i}}^{\star}(k)$ is the estimated set-point for the density at the bottleneck cell; and K_A is the controller gain, which can be defined, e.g., via a trial-and-error procedure. Note that, due to input saturation, the value $u(k-1)$ used in the right-hand side of (58) should be the bounded value of the previous time step, i.e., after application of the upper and lower bounds constraints (considering, e.g., $u^{\min}$ and $u^{\max}$ as the lower and upper bound, respectively, for the input $u(k)$) in order to avoid the wind-up phenomenon in the regulator.

Since ramp metering actions may create a queue outside the motorway network, we introduce the following dynamics for the (vertical) queue length $w(k)$ (in veh)

$$w(k+1) = w(k) + T\left(d(k) - u(k)\right), \tag{59}$$

where $d(k)$ is the on-ramp external demand during time interval $(k, k+1]$.

In addition, in the presented experiments (as well as in the majority of real-life situations), we assume that the ramp capacity is smaller than the mainstream one; in the opposite

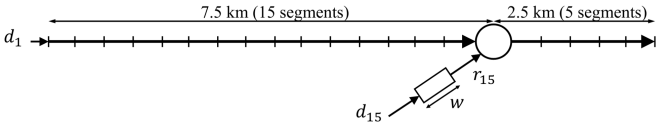

Fig. 4. The motorway stretch utilised in the simulation experiments.

case, there may be a need to consider the presence of on-ramp queues also for the no-control case, thus d should also be saturated.

C. Network Description and Simulation Configuration

We consider a two-lane motorway stretch, depicted in Fig. 4, which contains a metered on-ramp to test and evaluate the performance of the proposed strategy in the presence of changing FD. The stretch considered contains two origins, i.e., the main-stream and an on-ramp, two freeway links, and one destination. In particular, we consider a network composed of 20 segments of the same length $L_i = 0.5$ km, while we employ a time step $T = 10$ s. Typical ramp-metering implementations consider a control time-step in the order of 30–60 s [53]; thus, we update the control signal once in three simulation steps, i.e., the time-step of the controller is 30 s. The simulation horizon is 4 h, corresponding to $K = 1440$ steps.

We assume that the FD changes from FD_1 to FD_2 in the middle of our simulations (i.e., after 2 h, $k = 720$), which may reflect different traffic compositions (e.g., a high number of heavy vehicles altering the traffic characteristic of the motorway). We employ typical METANET parameters from [52], which are shown in Table I. Note that, in practice, the factual critical densities may not be the same as the values defined for the FD of the METANET model (i.e., the ones reported in Table I). This is due to the fact that, in second-order traffic models (such as METANET), the FD relation represents a "desired" target, which would happen only at steady-state, whereas traffic characteristics result from the dynamic model, where the actual speed is affected by the different terms in the speed dynamic equation (55) [54].

To examine the effects of the time-varying FD and the potential of ramp metering to mitigate congestion, we consider the following demand scenario (see also Fig. 5). The mainstream demand is kept constant at a relatively high level (about 80% of the nominal capacity) for the first 3 h of simulation, dropping to a low level (less than 50% of the nominal capacity) during the last hour; the latter being a cool-down period useful for ensuring that any congestion dissipates to allow fair numerical comparisons. The demand on the on-ramp increases for the first time after 10 min to a high value, remains constant for 30 min, and decreases to a constant low value. This is expected to create some congestion while traffic behaves according to FD_1. Then, after the FD changes to FD_2, the on-ramp demand increases for a second time, remains constant for 45 min, and finally decreases to a constant low value. This scenario is defined such that two independent congestion instances occur with different FDs.

We employ as performance metrics the Total Time Spent (TTS) and the Total Delay (TD) over a finite time horizon K;

TABLE I

PARAMETER VALUES USED IN THE NONLINEAR MULTI-LANE TRAFFIC FLOW MODEL (54)–(57)

	$v^{\text{max-min}}$ [km/h]	Q^{cap} [veh/h]	ρ^{cr} [veh/km]	ρ^{jam} [veh/km]	τ	ν	κ	δ	α
FD_1	107-7	2000	29	210	$\frac{20}{3600}$	35	13	0.8	2.2768
FD_2	107-7	1800	26	180	$\frac{20}{3600}$	35	13	0.8	2.2968

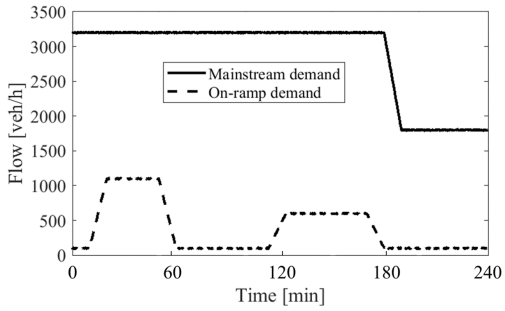

Fig. 5. Traffic demand used in the simulation experiments.

TTS is defined as

$$\text{TTS} = T \sum_{k=0}^{K} \sum_{i=0}^{N} \lambda_i L_i \rho_i(k) + T\, w(k), \tag{60}$$

which allows considering both the effects of congestion created in the mainstream and the queue generated at the on-ramp when ramp metering is implemented.

The TD can be computed as

$$\text{TD} = \text{TTS} - \text{TFFTT}, \tag{61}$$

where TFFTT is the Total Free Flow Travel Time, namely the total travel time that vehicles would experience if they were allowed to travel at the free flow speed. In order to calculate the TFFTT, we first introduce the Free Flow Travel Time, $\text{FFTT}_i(k)$, for a given link i at time k, which is

$$\text{FFTT}_i(k) = \frac{L_i}{v_i^{\text{free}}(k)}; \tag{62}$$

for each link and time, the number of vehicles experiencing such travel time is $q_i(k) \cdot T$; therefore the resulting TFFTT is

$$\begin{aligned} \text{TFFTT} &= \sum_k \sum_i \text{FFTT}_i(k) q_i(k) T \\ &= T \sum_k \sum_i q_i(k) \frac{L_i}{v_i^{\text{free}}(k)}. \end{aligned} \tag{63}$$

D. Reference Model Formulation

As discussed in Section II, the proposed estimator requires the definition of a reference model characterised by stable dynamics, where one of the states is the integral of the other state. Here, we employ the well-known mass-spring-damper model [55], which is a two-state system with globally stable dynamics. Actually, for each of the estimated $\hat{q}^\star$, or $\hat{\rho}^\star$ we are using an independent mass-spring-damper model; thus,

describing them in a single system, we employ a four-state system with stable states around r_e, defined as follows

$$\dot{X}_r = A_r X_r + B_r r_e \tag{64}$$

$$A_r = \begin{bmatrix} 0 & 1 & 0 & 0 \\ -K_r & -C_r & 0 & 0 \\ 0 & 0 & 0 & 1 \\ 0 & 0 & -K_r & -C_r \end{bmatrix}, \quad B_r = \begin{bmatrix} 0 & 0 \\ K_r & 0 \\ 0 & 0 \\ 0 & K_r \end{bmatrix}, \tag{65}$$

where $X_r := \left[\int \hat{q}^\star\, dt,\ \hat{q}^\star,\ \int \hat{\rho}^\star\, dt,\ \hat{\rho}^\star\right]^{\mathrm{T}}$, thus $X_M = \left[X_{r_{1,1}}\ X_{r_{3,1}}\right]^{\mathrm{T}}$ as $X_M \equiv X$ in (14), and $K_r > 0$ and $C_r > 0$ are the spring and damper coefficients, respectively. The system is globally stable to r_e as all the eigenvalues of A_r are negative and the pair (A_r, B_r) is stabilisable (see, e.g., [56]).

In the performed experiments, while applying control, we employ the feedback law (58) in the model (54)–(57). The controller gain is set as $K_A = 15$ (tuned via trial-and-error), while the set-point is determined via (52) iteratively calculating (50). A sensitivity analysis involving parameters K_r and C_r has been carried out, which is reported in Section IV-F (see also [29]); for our experiments, we use the following values: $K_r = 10$ and $C_r = 2$. Finally, the initial value of the growth rate in (51) is set as $\Gamma(0) = 10$, $\beta = 0.001$, and from (10) we know that $\Theta(B_e) = \begin{bmatrix} 1 & 1 \\ 0 & 1 \end{bmatrix}$.

IV. Experimental Results

We now proceed by presenting quantitative results demonstrating the performance of the proposed methodology for different settings of the proposed estimator. We define and consider the following baseline scenarios for our comparisons.

- **Scenario 1:** the no-control case, where the ramp flow is not metered, therefore congestion is expected to be formed;
- **Scenario 2:** a controlled case with known set-points, where ramp metering is active, considering that critical densities (thus, the set-points) are perfectly known (obtained, e.g., by analysing the no-control case results);
- **Scenario 3:** a controlled case where the set-point is maintained constant during the whole simulation. Here we test two different sub-scenarios: in the first sub-scenario, the set-point is set equal to the critical density employed for the first half of the simulation, i.e., according to FD_1 (Scenario 3-a); in the second sub-scenario, the set-point is set equal to the critical density employed for the second half of simulation, i.e., FD_2 (Scenario 3-b).

We reasonably expect that the no-control case (Scenario 1) is a lower bound for performance, while the controlled case with known set-points (Scenario 2) is an upper bound for the improvements that may be achieved. We then implement and evaluate controlled scenarios utilising our estimator as follows.

- **Scenario 4:** we test the estimator by setting as initial set-point the critical densities of FD_1 and FD_2, in Scenarios 4-a and 4-b, respectively;
- **Scenario 5:** we test our estimator by considering initial set-points values that are very high (Scenario 5-a) and very low (Scenario 5-b) compared to the actual ones.

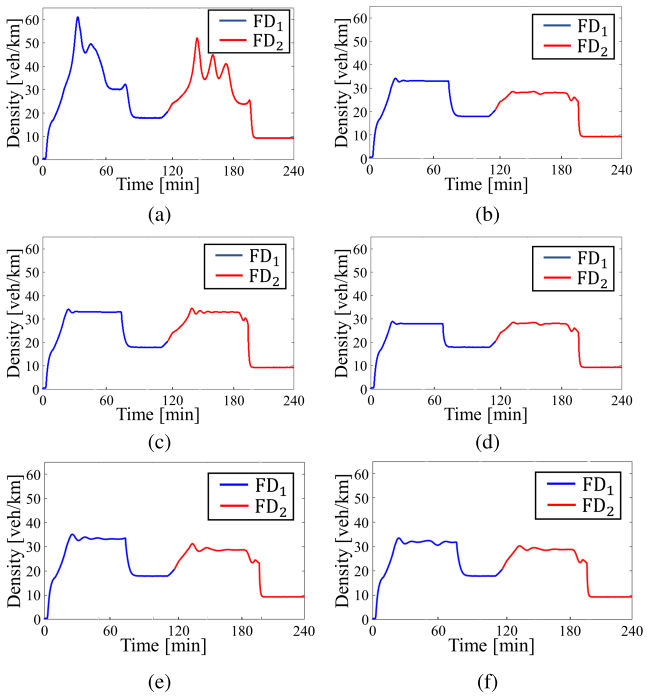

Fig. 6. Density of the bottleneck area: (a) Scenario 1. (b) Scenario 2. (c) Scenario 3-a. (d) Scenario 3-b. (e) Scenario 4-a. (f) Scenario 4-b.

In the plots presented afterwards, we use the blue colour for reporting the results of the FD employed during the first half of the simulation (FD_1) and the red colour for the FD employed during the second half of the simulation (FD_2).

A. Scenario 1: No-Control Case

The no-control case consists of the implementation of the nonlinear traffic model (54)–(57) in the presented motorway stretch, where no ramp metering is considered. According to Fig. 7(a), one may see that congestion occurs twice at the merging area (segment 15), which spills back upstream reaching up to segment 2, while the density at the bottleneck cell grows well above its critical value as it can be seen from Figs. 6(a) and 8(a). The congestion occurs due to the high inflow entering both the mainstream and the ramp, which exceeds the bottleneck capacity. In fact, during the first half of the simulation, when the bottleneck capacity is around 4000 veh/h, the total demand reaches 4300 veh/h; in the second half of the simulation, when the bottleneck capacity is around 3600 veh/h, the total demand reaches 3800 veh/h. Note that capacity drop also happens at the bottleneck cells of the stretch, which reduces capacity once congestion is set, with the consequence of intensifying the resulting congestion. The resulting TTS, calculated via (60), is reported in Table II

B. Scenario 2: Controlled Cases With Time-Varying Known Set-Points

Analysing the results of Section IV-A and, in particular, by looking at Fig. 8(a), which shows FD_1 (blue) and FD_2 (red) resulting from the no-control case, one may observe that the actual critical densities of the FDs, i.e., the densities corresponding to the maximum outflows are 33 veh/km and

TABLE II
TTS AND TD VALUE REPORT REGARDING THE DIFFERENT SCENARIOS

Case study	$\hat{\rho}^{\star}(0)$ [veh/km]	Online estimator	TTS [veh·h]		TTS improvement (%)		TD [veh·h]		TD improvement (%)	
Scenario 1	–	–	1690		–		579		–	
Scenario 2	–	Off	1583		6.3		387		33.1	
Scenario 3	(a): 33	Off	1624		3.9		512		11.6	
	(b): 28	Off	1635		3.1		525		9.1	
Method			Proposed method	Method in [45]	Proposed method	Method in [45]	Proposed method	Method in [45]	Proposed method	Method in [45]
Scenario 4	(a): 33	On	1590	1619	5.9	4.2	457	501	21.1	13.5
	(b): 28	On	1609	1631	4.8	3.5	473	513	18.3	11.4
Scenario 5	(a): 40	On	1619	1638	4.2	3.1	494	516	14.8	10.9
	(b): 20	On	1622	1678	4.0	2.5	503	520	13.1	10.1

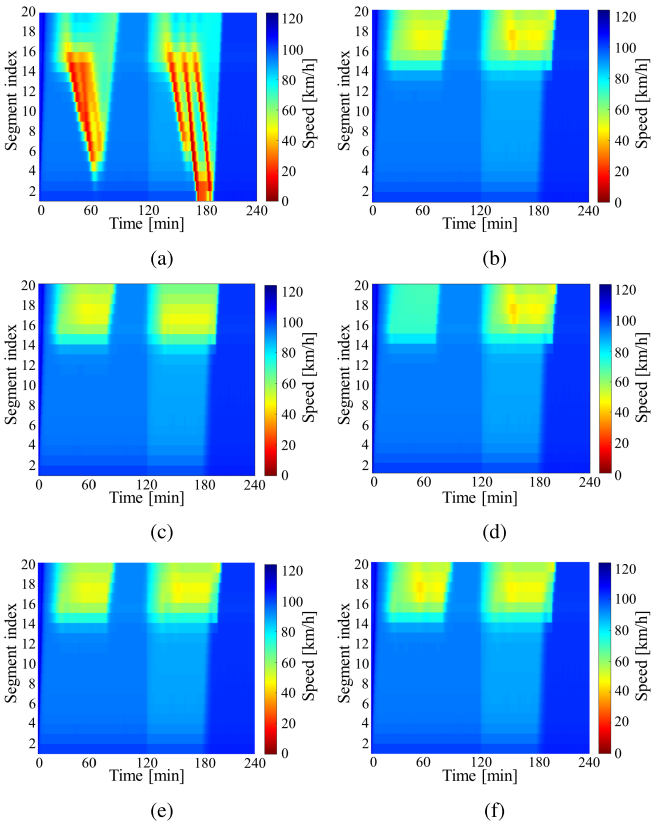

Fig. 7. Contour plots for speed: (a) Scenario 1. (b) Scenario 2. (c) Scenario 3-a. (d) Scenario 3-b. (e) Scenario 4-a. (f) Scenario 4-b.

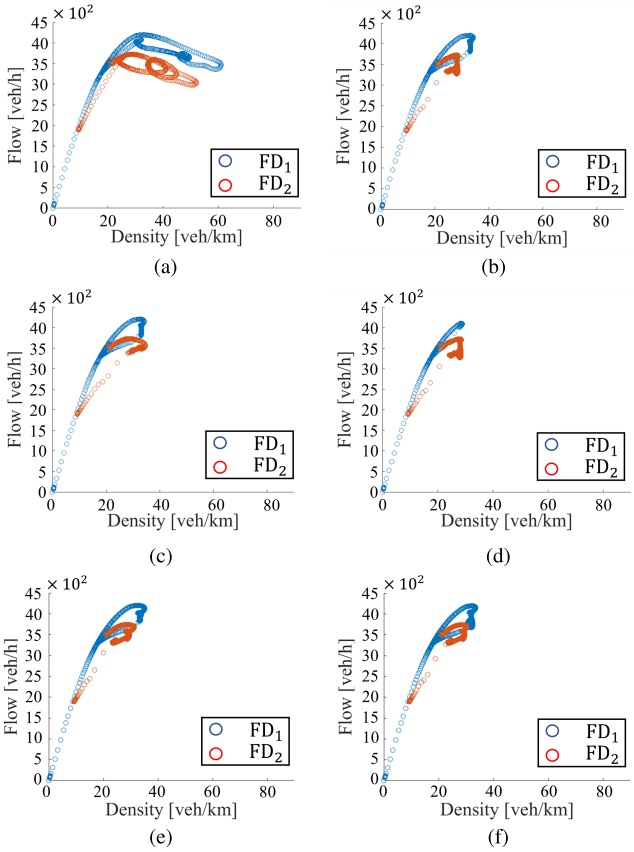

Fig. 8. Fundamental Diagram: (a) Scenario 1. (b) Scenario 2. (c) Scenario 3-a. (d) Scenario 3-b. (e) Scenario 4-a. (f) Scenario 4-b.

28 veh/km for FD_1 and FD_2, respectively. These values are the ones employed for the controlled case with known set-points.

Then, we evaluate the performance achievable by controlling the traffic via ramp metering, assuming that we have perfect knowledge of the critical densities (thus, the set-points) in real-time. Note that this corresponds to an unrealistic scenario, as the actual critical densities cannot be observed unless we are reaching a (nearly) congested state. Still, it is interesting to perform such an experiment, in order to determine an upper bound for the performance of our estimation strategy.

We therefore implement the nonlinear traffic model (54)–(57), where the on-ramp flow is calculated via (58), while $\hat{\rho}^{\star}(k) = 33$ veh/km for $0 \leq k < 720$ and $\hat{\rho}^{\star}(k) = 28$ veh/km for $720 \leq k \leq 1440$.

The results in Figs. 6(b), 7(b), and 8(b) show that congestion disappears and the bottleneck cell's density is maintained around its critical value for both FD_1 and FD_2. To assess the controller performance numerically, we compare the TTS and TD, reported in Table II, where one may see that Scenario 2 results in a 6.3% for TTS improvement and 33.1% for TD improvement over the no-control case in Scenario 1. Furthermore, queues are generated at the on-ramps during the peak periods in all controlled scenarios; note that no upper bound for the queue length is considered in our experiments.

C. Scenario 3: Controlled With Constant Set-Points

In this scenario, we apply ramp metering employing a constant set-point during the simulation. Basically, this scenario represents what is typically done in existing ramp metering applications, where the set-point is estimated from historical data and maintained constant during implementation. In particular, we test two sub-scenarios, one (Scenario 3-a) using as a set-point the critical density of FD_1 and another one (Scenario 3-b) using as a set-point the critical density of FD_2. That is, we implement the nonlinear traffic model (54)–(57), where the on-ramp flow is calculated via (58), where, in Scenario 3-a, $\hat{\rho}^\star(k) = 33$ veh/km, $\forall k$; and, in Scenario 3-b, $\hat{\rho}^\star(k) = 28$ veh/km, $\forall k$.

Results in Fig. 6(c,d) show that the congestion is mitigated in both sub-scenarios. According to Figs. 7(c,d) and Figs. 8(c,d), we observe that, for all sub-scenarios, the controller is capable to maintain the bottleneck cell's density around the desired set-point during the period characterised by high demand for both FD_1 to FD_2. However, as these values do not maximise the throughput for some time, numerical comparisons presented in Table II reveal that the controller is capable to achieve only 3.9% and 3.1% for TTS improvement, and 11.6% and 9.1% for TD improvement compared to the no-control case for Scenarios 3-a and 3-b, respectively. Also in this case, we show in Fig. 9(b,c) the generated queues at the on-ramp location regarding Scenario 3-a and 3-b, which shows a slight queue length reduction compared to Scenario 2, especially regarding FD_2.

D. Scenario 4: Controlled With Estimated Set-Points

We proceed then with evaluating the performance of our estimator, by considering two sub-scenarios considering different initial values for the estimated set-points, corresponding to the critical densities of FD_1 and FD_2. We implement the nonlinear traffic model (54)–(57), where the on-ramp flow is calculated via (58), and $\hat{\rho}^\star(k)$ and $\hat{\rho}^\star(k)$ are estimated via (52) and (53) respectively. We test Scenario 4-a, where $\hat{\rho}^\star(0) = 33$ veh/km, and Scenario 4-b, where $\hat{\rho}^\star(0) = 28$ veh/km.

Looking at the results regarding Scenario 4-a, as shown in Figs. 6(e), 7(e), and 8(e), we observe that the controller with the estimator is capable of avoiding the onset of congestion, similarly to the other controlled scenarios. Moreover, we can also see that the estimator manages to successfully adjust set-point values to the actual critical values, while successfully controlling the system. This is also shown in more detail in Fig. 10(b), where the estimated critical density settles to the actual value around $t = 150$ min, i.e., 30 minutes after the change in the FD. In addition, Fig. 10(a) shows the estimated maximum outflow, where the changes start earlier than the estimated density ($t = 100$ min). Numerical comparisons in terms of TTS, reported in Table II, demonstrate that utilising the estimator not only improves traffic conditions compared to the control case (Scenario 1) but also outperforms all the scenarios where a constant set-point is used; for example, the TTS improvement and TD improvement in Scenario 4-a are 51% and 81% higher than in Scenario 3-a, respectively. In addition, queues resulting from Scenario 4-a are generated

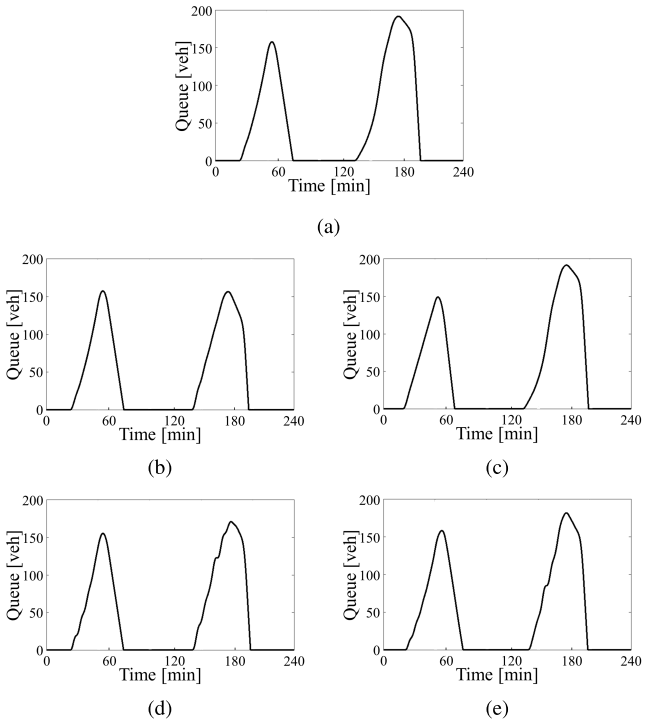

Fig. 9. Ramp queue: (a) Scenario 2. (b) Scenario 3-a. (c) Scenario 3-b. (d) Scenario 4-a. (e) Scenario 4-b.

at the on-ramp location during the peak periods, for which no upper-bound is considered in our experiments (see Fig. 9(c,d)).

Similarly, in Scenario 4-b the controller manages to avoid the congestion successfully, as can be seen from Figs. 6(f), 7(f), and 8(f). In particular, as shown in Fig. 6(f), the estimator successfully adjusts set-point values to the critical density after the FD changes. This is shown in more detail in Fig. 10(d), where the estimated critical density reaches first, at $t = 16$ min, 33 veh/km and then, around $t = 140$ min, 28 veh/km. In addition, Fig. 10(c) reveals the estimated maximum outflow, where the convergence to its true value starts earlier than the estimated density ($t = 100$ min). Also for this Scenario, the resulting TTS and TD are lower than in the no-control case and than any controlled Scenario with a constant set-point; in particular, the TTS improvement and TD improvement in Scenario 4-b are 54% and 58% higher than in Scenario 3-b, respectively. Also in this case, we show in Fig. 9(e) the generated queues at the on-ramp location regarding Scenario 4-b. According to this figure, the estimator could slightly reduce the queue compared to Scenario 3, especially for FD_2.

E. Scenario 5: Controlled With Estimated Set-Points and Distant Initial Values

In this scenario, we investigate the performance of the controller with the adaptive estimator in two cases, where the initial values of the set-points are distant from the actual values, utilising in particular (a) a very high value (Scenario 5-a), i.e., $\hat{\rho}^\star(0) = 40$ veh/km, and (b) a very low value (Scenario 5-b), i.e., $\hat{\rho}^\star(0) = 20$ veh/km.

Looking at Figs 11(a,b), we observe that the densities at the bottleneck area are maintained around their true critical values

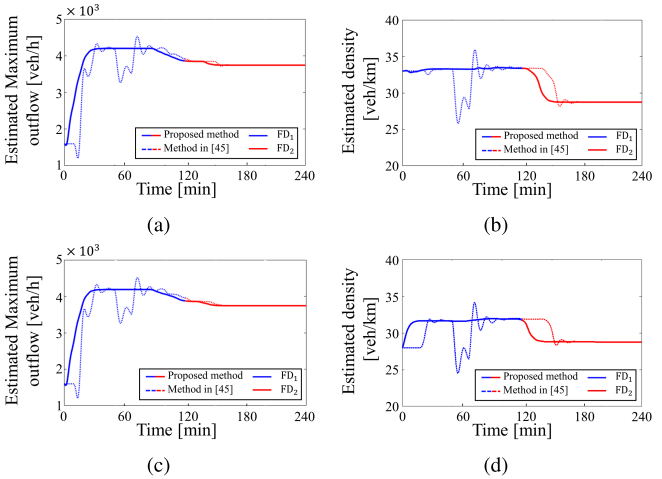

Fig. 10. Estimated values, left: maximum out flow ($q^\star$), right: Critical density ($\rho^\star$), for: (a,b) Scenario 4-a, where $\hat{\rho}^\star(0) = 33$ veh/km. (c,d) Scenario 4-b, where $\hat{\rho}^\star(0) = 28$ veh/km.

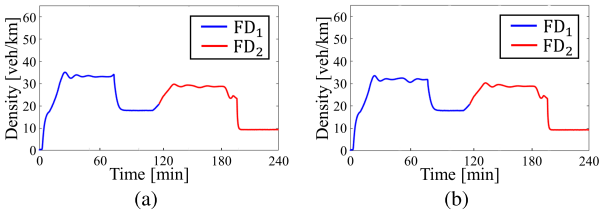

Fig. 11. Density of the bottleneck areas for: (a) Scenario 5-a, where $\hat{\rho}^\star(0) = 40$ veh/km. (b) Scenario 5-b, where $\hat{\rho}^\star(0) = 20$ veh/km.

for both Scenarios 5-a and 5-b, although the initial conditions are considerably far from the actual values. This demonstrates that the proposed estimator is capable of achieving a proper convergence in a short time. In particular, we can see from Figs. 12(b,d) that, for both Scenarios 5-a and 5-b, the estimator reaches the actual set-point value ($\rho^\star = 33$ veh/km) around $t = 25$ min, while Figs. 12(a,c) show that the maximum outflow ($\hat{q}^\star$) is also properly estimated.

Also for this Scenario, the TTS and TD values are reported in Table II, where we can see that the percentage of improvement is 4.2% and 4.0% for TTS, and 14.8% and 13.1% for TD, respectively, compared to the no-control case (Scenario 1), thus outperforming Scenario 3.

F. Sensitivity Analysis of the Reference Model Parameters

Although the reference model defined in Section III-D is proven to be globally stable, which guarantees the convergence of the estimated parameters, the quality and speed of the estimation process may be affected by a proper choice of the parameters K_r and C_r. In order to investigate their effect, we perform a set of experiments considering Scenario 4, as introduced in Section IV-D, comparing the resulting TTS to better understand the sensitivity of the convergence process and tracking error to the choice of such parameters. The results are reported in Fig. 13, where one may observe that the ranges of K_r and C_r that produce positive effects in terms of TTS improvement (i.e., the orange area) are very wide, that is, the estimator is not very sensitive to such parameters choice while we remain within these ranges. Still, one may observe a darker

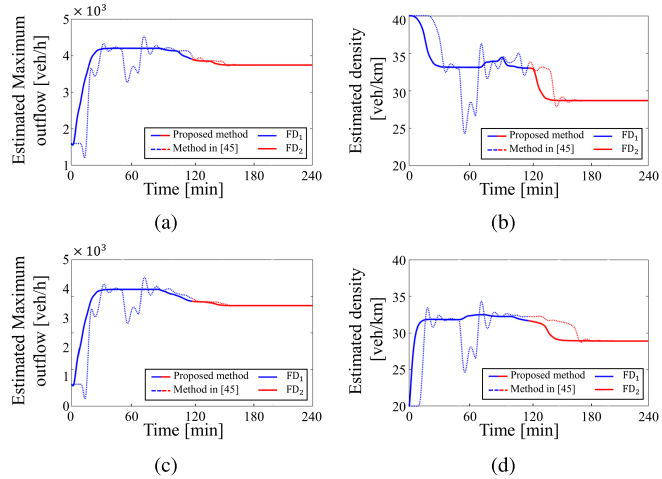

Fig. 12. Estimated values, left: maximum outflow ($q^\star$), right: Critical density ($\rho^\star$) for (a,b) Scenario 5-a, where $\hat{\rho}^\star(0) = 40$ veh/km. (c,d) Scenario 5-b, where $\hat{\rho}^\star(0) = 20$ veh/km.

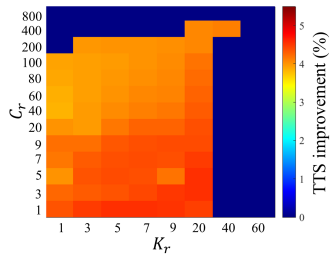

Fig. 13. Sensitivity analysis showing the percentage of TTS improvement compared to the no-control case for a domain of K_r and C_r.

orange area, where $1 \leq K_r \leq 20$, and $1 \leq C_r \leq 9$, which leads to the best performance in terms of TTS improvement. Thus, for our experiments, we select $K_r = 10$, and $C_r = 2$, which lie in this area with the highest TTS improvement value.

G. Comparisons With Existing Methods

To investigate the numerical improvements achieved with respect to the method proposed in [45], we implement such a method in the same simulation scenarios presented above, while the results are reported in Table II, and the quality of estimation is shown in Figs. 10 and 12. Looking at Figs. 10(b,d) and 12(b,d), one can observe that the estimator in [45] features stronger oscillations and generally has a higher delay in converging to the true critical density value compared to the proposed method (on average, around 20 min). The oscillations are due to the choice of a conditionally stable Lyapunov function used to develop the adaptation law, while in the proposed version the oscillations are minimal as we develop the adaptation rule based on the global exponential stable Lyapunov function (21). In addition, the delay is expected for the method in [45] because of the designed small value for the growth rate, while, in the proposed version, the growth rate in (32) can vary depending on the stability conditions for the estimator error ($\hat{\Pi} \rightarrow \Pi$). Finally, from Table II, it can be observed that the proposed method outperforms the method [45] for all scenarios, in terms of both TTS and TD improvement, by an average of 42% and 46%, respectively.

V. Conclusion

This paper proposed a novel robust adaptive estimator to estimate the set-point values (i.e., critical density) for local traffic control strategies, designed to achieve maximum throughput at a bottleneck area, assuming the FD is unknown and time-varying. The global asymptotical stability of the estimator is proven through a Lyapunov function, guaranteeing convergence to the actual critical density and maximum outflow. In addition, the stability and convergence of the estimator's parameters are investigated via a least-square method. We implemented the controller and the estimator with the feedback controller for ramp metering ALINEA, utilising the traffic flow model METANET modified to account for a time-varying FD. Our numerical results show that employing the adaptive estimator outperforms the ALINEA controller in terms of TTS in case a constant set-point is utilised. Furthermore, to assess the robustness of the estimator, we tested extreme cases for the initial estimates.

Further developments include the incorporation in the control strategy of mainstream flow control, which may be implemented, for example, via variable speed limits, as well as accounting for the presence of multiple bottlenecks; the latter could, e.g., follow the works in [57] and [58]. Another possible direction is to investigate the case of more complex networks, characterised by multiple destinations, where, e.g., the behaviour of CAVs is defined per destination.

References

[1] J. Rios-Torres and A. A. Malikopoulos, "A survey on the coordination of connected and automated vehicles at intersections and merging at highway on-ramps," *IEEE Trans. Intell. Transp. Syst.*, vol. 18, no. 5, pp. 1066–1077, May 2017.

[2] F. Tajdari, "Optimal and adaptive controller design for motorway traffic with connected and automated vehicles," Doctoral thesis, School Eng., Aalto Univ., Espoo, Finland, 2023. [Online]. Available: http://urn.fi/URN:ISBN:978-952-64-1102-6

[3] X. Yang, Y. Xu, L. Kuang, Z. Wang, H. Gao, and X. Wang, "An information fusion approach to intelligent traffic signal control using the joint methods of multiagent reinforcement learning and artificial intelligence of things," *IEEE Trans. Intell. Transp. Syst.*, vol. 23, no. 7, pp. 9335–9345, Jul. 2022.

[4] K. Chung, J. Rudjanakanoknad, and M. J. Cassidy, "Relation between traffic density and capacity drop at three freeway bottlenecks," *Transp. Res. B, Methodol.*, vol. 41, no. 1, pp. 82–95, 2007.

[5] K. Kim and M. J. Cassidy, "A capacity-increasing mechanism in freeway traffic," *Transp. Res. B, Methodol.*, vol. 46, no. 9, pp. 1260–1272, Nov. 2012.

[6] H. Y. Jin and W. L. Jin, "Control of a lane-drop bottleneck through variable speed limits," *Transp. Res. C, Emerg. Technol.*, vol. 58, pp. 568–584, Sep. 2015.

[7] M. Papageorgiou, C. Diakaki, V. Dinopoulou, A. Kotsialos, and Y. Wang, "Review of road traffic control strategies," *Proc. IEEE*, vol. 91, no. 12, pp. 2043–2067, Dec. 2003.

[8] F. Tajdari, A. Golgouneh, A. Ghaffari, A. Khodayari, A. Kamali, and N. Hosseinkhani, "Simultaneous intelligent anticipation and control of follower vehicle observing exiting lane changer," *IEEE Trans. Veh. Technol.*, vol. 70, no. 9, pp. 8567–8577, Sep. 2021.

[9] M. Papageorgiou, H. Hadj-Salem, and J.-M. Blosseville, "ALINEA: A local feedback control law for on-ramp metering," *Transp. Res. Rec.*, vol. 1320, pp. 58–64, Jan. 1991.

[10] P. Kachroo, L. Ratliff, and S. Sastry, "Analysis of the Godunov-based hybrid model for ramp metering and robust feedback control design," *IEEE Trans. Intell. Transp. Syst.*, vol. 15, no. 5, pp. 2132–2142, Oct. 2014.

[11] S. Agarwal, P. Kachroo, S. Contreras, and S. Sastry, "Feedback-coordinated ramp control of consecutive on-ramps using distributed modeling and Godunov-based satisfiable allocation," *IEEE Trans. Intell. Transp. Syst.*, vol. 16, no. 5, pp. 2384–2392, Oct. 2015.

[12] C. Pasquale, S. Sacone, S. Siri, and A. Ferrara, "Hierarchical centralized/decentralized event-triggered control of multiclass traffic networks," *IEEE Trans. Control Syst. Technol.*, vol. 29, no. 4, pp. 1549–1564, Jul. 2021.

[13] R. C. Carlson, I. Papamichail, and M. Papageorgiou, "Local feedback-based mainstream traffic flow control on motorways using variable speed limits," *IEEE Trans. Intell. Transp. Syst.*, vol. 12, no. 4, pp. 1261–1276, Dec. 2011.

[14] J. R. D. Frejo and B. De Schutter, "Logic-based traffic flow control for ramp metering and variable speed limits—Part 1: Controller," *IEEE Trans. Intell. Transp. Syst.*, vol. 22, no. 5, pp. 2647–2657, May 2021.

[15] L. Zhu, L. Lu, X. Wang, C. Jiang, and N. Ye, "Operational characteristics of mixed-autonomy traffic flow on the freeway with on- and off-ramps and weaving sections: An RL-based approach," *IEEE Trans. Intell. Transp. Syst.*, vol. 23, no. 8, pp. 13512–13525, Aug. 2022.

[16] Z. Gao, Z. Wu, W. Hao, K. Long, Y.-J. Byon, and K. Long, "Optimal trajectory planning of connected and automated vehicles at on-ramp merging area," *IEEE Trans. Intell. Transp. Syst.*, vol. 23, no. 8, pp. 12675–12687, Aug. 2022.

[17] S. Sharma, I. Papamichail, A. Nadi, H. Van Lint, L. Tavasszy, and M. Snelder, "A multi-class lane-changing advisory system for freeway merging sections using cooperative ITS," *IEEE Trans. Intell. Transp. Syst.*, vol. 23, no. 9, pp. 15121–15132, Sep. 2022.

[18] M. A. Silgu, I. G. Erdagi, G. Goksu, and H. B. Celikoglu, "Combined control of freeway traffic involving cooperative adaptive cruise controlled and human driven vehicles using feedback control through SUMO," *IEEE Trans. Intell. Transp. Syst.*, vol. 23, no. 8, pp. 11011–11025, Aug. 2022.

[19] T. Yuan, F. Alasiri, and P. A. Ioannou, "Selection of the speed command distance for improved performance of a rule-based VSL and lane change control," *IEEE Trans. Intell. Transp. Syst.*, vol. 23, no. 10, pp. 19348–19357, Oct. 2022.

[20] H. Liu, C. G. Claudel, R. Machemehl, and K. A. Perrine, "A robust traffic control model considering uncertainties in turning ratios," *IEEE Trans. Intell. Transp. Syst.*, vol. 23, no. 7, pp. 6539–6555, Jul. 2022.

[21] H. Liu, C. Claudel, and R. Machemehl, "Robust traffic control using a first order macroscopic traffic flow model," *IEEE Trans. Intell. Transp. Syst.*, vol. 23, no. 7, pp. 8048–8062, Jul. 2022.

[22] R. Bishop, *Intelligent Vehicle Technology and Trends*. Norwood, MA, USA: Artech House, 2005.

[23] C. Diakaki, M. Papageorgiou, I. Papamichail, and I. Nikolos, "Overview and analysis of vehicle automation and communication systems from a motorway traffic management perspective," *Transp. Res. A, Policy Pract.*, vol. 75, pp. 147–165, May 2015.

[24] C. Roncoli, M. Papageorgiou, and I. Papamichail, "Traffic flow optimisation in presence of vehicle automation and communication systems—Part II: Optimal control for multi-lane motorways," *Transp. Res. C, Emerg. Technol.*, vol. 57, pp. 260–275, Aug. 2015.

[25] Y. Zhang and P. A. Ioannou, "Combined variable speed limit and lane change control for highway traffic," *IEEE Trans. Intell. Transport. Syst.*, vol. 7, pp. 1812–1823, 2017.

[26] I. Papamichail et al., "Motorway traffic flow modelling, estimation and control with vehicle automation and communication systems," *Annu. Rev. Control*, vol. 48, pp. 325–346, Jan. 2019.

[27] A. Kouvelas, K. Aboudolas, E. Kosmatopoulos, and M. Papageorgiou, "Adaptive performance optimization for large-scale traffic control systems," *IEEE Trans. Intell. Transp. Syst.*, vol. 12, no. 4, pp. 1434–1445, Apr. 2008.

[28] R. Kutadinata, W. Moase, C. Manzie, L. Zhang, and T. Garoni, "Enhancing the performance of existing urban traffic light control through extremum-seeking," *Transp. Res. C, Emerg. Technol.*, vol. 62, pp. 1–20, Jan. 2016.

[29] F. Tajdari, C. Roncoli, and M. Papageorgiou, "Feedback-based ramp metering and lane-changing control with connected and automated vehicles," *IEEE Trans. Intell. Transp. Syst.*, vol. 23, no. 2, pp. 939–951, Feb. 2022.

[30] K. B. Ariyur and M. Krstic, *Real-Time Optimization by Extremum-Seeking Control*. Hoboken, NJ, USA: Wiley, 2003.

[31] D. M. Bramich, M. Menendez, and L. Ambuhl, "Fitting empirical fundamental diagrams of road traffic: A comprehensive review and comparison of models using an extensive data set," *IEEE Trans. Intell. Transp. Syst.*, vol. 23, no. 9, pp. 14104–14127, Sep. 2022.

[32] X. Shi and X. Li, "Constructing a fundamental diagram for traffic flow with automated vehicles: Methodology and demonstration," *Transp. Res. B, Methodol.*, vol. 150, pp. 279–292, Aug. 2021.

[33] H. Yu, S. Koga, T. R. Oliveira, and M. Krstic, "Extremum seeking for traffic congestion control with a downstream bottleneck," *J. Dyn. Syst., Meas., Control*, vol. 143, no. 3, Mar. 2021, Art. no. 031007.
[34] E. Kosmatopoulos et al., "Real-time estimation of critical occupancy for maximum motorway throughput," *Transp. Res. Rec., J. Transp. Res. Board*, vol. 1959, no. 1, pp. 65–76, Jan. 2006.
[35] T. R. Oliveira, M. Krstić, and D. Tsubakino, "Extremum seeking for static maps with delays," *IEEE Trans. Autom. Control*, vol. 62, no. 4, pp. 1911–1926, Apr. 2017.
[36] J.-J. E. Slotine and W. Li, *Applied Nonlinear Control*, vol. 199. Englewood Cliffs, NJ, USA: Prentice-Hall, 1991.
[37] H. Jin, Z. Liu, H. Zhang, Y. Liu, and J. Zhao, "A dynamic parameter identification method for flexible joints based on adaptive control," *IEEE/ASME Trans. Mechatronics*, vol. 23, no. 6, pp. 2896–2908, Dec. 2018.
[38] J. E. Gaudio, A. M. Annaswamy, E. Lavretsky, and M. A. Bolender, "Parameter estimation in adaptive control of time-varying systems under a range of excitation conditions," *IEEE Trans. Autom. Control*, vol. 67, no. 10, pp. 5440–5447, Oct. 2022.
[39] F. Tajdari and N. E. Toulkani, "Implementation and intelligent gain tuning feedback-based optimal torque control of a rotary parallel robot," *J. Vibrat. Control*, vol. 28, nos. 19–20, pp. 2678–2695, Oct. 2022.
[40] S. Wang and J. Na, "Parameter estimation and adaptive control for servo mechanisms with friction compensation," *IEEE Trans. Ind. Informat.*, vol. 16, no. 11, pp. 6816–6825, Nov. 2020.
[41] J. Haddad and Z. Zheng, "Adaptive perimeter control for multi-region accumulation-based models with state delays," *Transp. Res. B, Methodol.*, vol. 137, pp. 133–153, Jul. 2020.
[42] J. Haddad and B. Mirkin, "Coordinated distributed adaptive perimeter control for large-scale urban road networks," *Transp. Res. C, Emerg. Technol.*, vol. 77, pp. 495–515, Apr. 2017.
[43] J. Haddad and B. Mirkin, "Adaptive tracking of uncertain nonlinear systems under different types of input delays with urban traffic perimeter control application," *Int. J. Robust Nonlinear Control*, vol. 31, no. 15, pp. 6975–6990, Oct. 2021.
[44] J. Haddad and B. Mirkin, "Adaptive perimeter traffic control of urban road networks based on MFD model with time delays," *Int. J. Robust Nonlinear Control*, vol. 26, no. 6, pp. 1267–1285, Apr. 2016.
[45] F. Tajdari and C. Roncoli, "Adaptive traffic control at motorway bottlenecks with time-varying fundamental diagram," *IFAC-PapersOnLine*, vol. 54, no. 2, pp. 271–277, 2021.
[46] M. Papageorgiou and A. Kotsialos, "Freeway ramp metering: An overview," *IEEE Trans. Intell. Transp. Syst.*, vol. 3, no. 4, pp. 271–281, Apr. 2002.
[47] A. Visioli, *Practical PID Control*. Berlin, Germany: Springer, 2006.
[48] H. K. Khalil, *Nonlinear Control*, vol. 406. New York, NY, USA: Pearson, 2015.
[49] F. Tajdari, T. Huysmans, Y. Yang, and Y. Song, "Feature preserving non-rigid iterative weighted closest point and semi-curvature registration," *IEEE Trans. Image Process.*, vol. 31, pp. 1841–1856, 2022.
[50] B. D. O. Anderson, "Exponential stability of linear equations arising in adaptive identification," *IEEE Trans. Autom. Control*, vol. AC-22, no. 1, pp. 83–88, Feb. 1977.
[51] A. P. Morgan and K. S. Narendra, "On the uniform asymptotic stability of certain linear nonautonomous differential equations," *SIAM J. Control Optim.*, vol. 15, no. 1, pp. 5–24, Jan. 1977.
[52] A. Messmer and M. Papageorgiou, "METANET: A macroscopic simulation program for motorway networks," *Traffic Eng. Control*, vol. 9, pp. 466–470, 1990.
[53] C. Wang, Y. Xu, J. Zhang, and B. Ran, "Integrated traffic control for freeway recurrent bottleneck based on deep reinforcement learning," *IEEE Trans. Intell. Transp. Syst.*, vol. 23, no. 9, pp. 15522–15535, Sep. 2022.
[54] M. Papageorgiou, J.-M. Blosseville, and H. Hadj-Salem, "Modelling and real-time control of traffic flow on the southern part of Boulevard Peripherique in Paris: Part I: Modelling," *Transp. Res. A, Policy Pract.*, vol. 24, no. 5, pp. 345–359, Sep. 1990.
[55] S. Armaghan, A. Moridi, and A. K. Sedigh, "Design of a switching PID controller for a magnetically actuated mass spring damper," in *Proc. World Congr. Eng.*, vol. 3, 2011, pp. 6–8.
[56] R. L. Williams and D. A. Lawrence, *Linear State-Space Control Systems*. Hoboken, NJ, USA: Wiley, 2007.
[57] Y. Wang, M. Papageorgiou, J. Gaffney, I. Papamichail, G. Rose, and W. Young, "Local ramp metering in random-location bottlenecks downstream of metered on-ramp," *Transp. Res. Rec.*, vol. 2178, pp. 90–100, Dec. 2010.
[58] G.-R. Iordanidou, C. Roncoli, I. Papamichail, and M. Papageorgiou, "Feedback-based mainstream traffic flow control for multiple bottlenecks on motorways," *IEEE Trans. Intell. Transp. Syst.*, vol. 16, no. 2, pp. 610–621, Apr. 2015.

Farzam Tajdari received the M.Sc. degree in mechanical engineering from the Amirkabir University of Technology, Tehran, Iran, in 2016, and the Ph.D. degree from Aalto University, Finland, in 2023. He is currently a Post-Doctoral Researcher with the Mechanical Engineering Department, TU Eindhoven. He is also working on autonomous and connected vehicles. His research interests include control, optimization, and non-linear systems to solve challenges in the fields of intelligent transportation systems, privacy of dynamic systems, and geometry processing.

Claudio Roncoli received the Ph.D. degree from the University of Genova, Italy, in 2013. He is currently an Associate Professor in transportation engineering with Aalto University, Finland. Before joining Aalto University in 2016, he was a Research Assistant with the University of Genova, a Visiting Research Assistant with the Imperial College London, U.K., and a Post-Doctoral Researcher with the Technical University of Crete, Greece. He has been involved in several national and international research projects as a principal investigator. His research interests include real-time traffic management, modeling, optimization, control of traffic systems with connected and automated vehicles, and smart mobility and intelligent transportation systems. Among other editorial duties, he serves as an Associate Editor for the IEEE TRANSACTIONS ON INTELLIGENT TRANSPORTATION SYSTEMS. He is also an Editorial Board Member of *Transportation Research Part C: Emerging Technologies*.